Modelling of macroscopic magnetic islands in tokamaks

F. Porcelli[a,b], A. Airoldi[c], C. Angioni[d], A. Bruschi[c], P. Buratti[e], F. Califano[f], S. Cirant[c], I. Furno[d], D. Grasso[a], E. Lazzaro[c], A.A. Martynov[d], M. Ottaviani[g], F. Pegoraro[f], G. Ramponi[c], E. Rossi[h], O. Sauter[d], C. Tebaldi[i], O. Tudisco[e]

[a] Istituto Nazionale Fisica della Materia and Dipartimento di Energetica, Politecnico di Torino, Turin, Italy

[b] Plasma Science and Fusion Center, Massachusetts Institute of Technology, Cambridge, Massachusetts, United States of America

[c] Istituto di Fisica del Plasma, Associazione Euratom–ENEA–CNR, Milan, Italy

[d] Centre de Recherches en Physique des Plasmas, Association Euratom–Confédération Suisse, Ecole Polytechnique Fédérale de Lausanne, Lausanne, Switzerland

[e] Associazione Euratom–ENEA sulla Fusione, Centro Ricerche Energia Frascati, Frascati, Italy

[f] Istituto Nazionale Fisica della Materia and Dipartimento di Fisica, Università degli Studi di Pisa, Pisa, Italy

[g] Département de Recherches sur la Fusion Contrôlée, CEA Cadarache, Saint-Paul-lez-Durance, France

[h] Institute for Fusion Studies, University of Texas at Austin, Austin, Texas, United States of America

[i] Dipartimento di Mathematica, Università di Lecce, Lecce, Italy

Abstract. The article presents experimental and theoretical investigations on the dynamics of sawteeth and neoclassical tearing modes in tokamak plasmas. The main findings of these investigations are: (1) The experimental validation, on the basis of FTU and TCV data, of a model for the prediction of the sawtooth period and amplitude; (2) the importance of diamagnetic effects in determining the threshold for sawtooth crashes and the rotation of non-linear tearing modes; (3) a clarification of collisionless reconnection processes, in particular the role of phase mixing in association with magnetic island growth and saturation in dissipationless regimes. The interplay between ECRH and macroscopic island dynamics is also discussed.

1. Introduction and the diamagnetic rotation of magnetic islands

Often the confinement properties of tokamak plasmas are limited by the onset of macroscopic, coherent magnetic islands. The qualification 'coherent' refers to single-helicity islands where chaotic field line behaviour does not play an important role. Typically, coherent islands correspond to magnetic perturbations with low poloidal mode numbers, such as neoclassical tearing modes and $m = 1$ resistive kinks. The non-linear evolution of these islands is still an open problem.

Diamagnetic effects are known to influence significantly the reconnecting magnetic instabilities. The important changes to the classic resistive tearing mode occur in the 'drift tearing regime' [1], when the electron diamagnetic frequency ω_{*e} is

sufficiently larger than the (normalized) growth rate [2], $\gamma_T = 0.55(\Delta')^{4/5}\eta^{3/5}$, obtained by the resistive MHD (RMHD) model, which ignores the equilibrium pressure gradients. For values of ω_{*e}/γ_T exceeding a critical threshold, the eigenfunction undergoes a transition to a radially oscillating, delocalized mode. One can construct an initially localized wave packet, which propagates outwards, undergoing spatial amplification. Furthermore, the nominal mode growth rate, which is obtained from the dispersion relation ignoring the localization problem, is strongly suppressed at high ω_{*e}/γ_T. A localized mode can be found when additional physics is included in the models. An important localizing non-dissipative effect, which can lead to the complete stabilization of the drift tearing mode, is the finite β coupling to sound waves [3]. Localization is also achieved by the introduction of appropriate dissipative or finite Larmor radius effects. The roles of two such effects, ion viscosity and particle diffusivity, are discussed in this section.

Diamagnetic effects are altered in the non-linear regime, as density and temperature profiles tend to flatten, on average, across the island region. This leads to two main questions: (i) To what extent are the stabilizing diamagnetic effects suppressed in the non-linear saturated regime? (ii) What are the actual mode structure and rotation frequency of saturated islands? These questions are especially relevant when treating more general models that predict full linear stability, as in Ref. [3], when one can argue that the non-linear suppression of the diamagnetic effects could lead to bistability, that is, the coexistence of states with and without magnetic islands for the same set of parameters.

In order to address these issues, we consider the three field non-linear version of the model of Ref. [1], with the inclusion of ion viscosity and particle diffusivity. The cold ion limit is taken for simplicity and the electron temperature is constant. The (suitably normalized) vorticity equation is

$$dU/dt = [J, \psi] + \mu\nabla^2 U \tag{1}$$

where ϕ is the electric potential, $U = \nabla^2\phi$, ψ is the magnetic flux function, $J = -\nabla^2\psi$ is the current density, $[A, B] \equiv (\partial_x A)(\partial_y B) - (\partial_x B)(\partial_y A)$, $d/dt \equiv \partial/\partial t + [\phi, \cdot]$, and μ is the ion viscosity coefficient. The Prandtl number is $P = \mu/\eta$. We adopt Ohm's law

$$d\psi/dt + v_*\partial_y\psi = [n, \psi] - \eta(J - J_{eq}) \tag{2}$$

where v_* is proportional to the equilibrium density gradient and η is the normalized electrical resistivity,

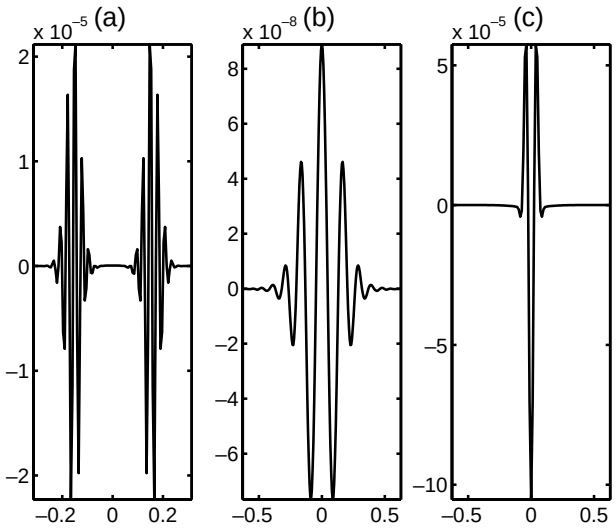

Figure 1. Perturbed current density. (a) Non-localized structure, $P = D = 0$; (b) viscosity localization, $P = 0.1$, $D = 0$; (c) diffusivity localization, $D = 0.01\eta$, $P = 0$.

while the fluctuating density n obeys the continuity equation

$$dn/dt + v_*\partial_y\phi = D\nabla^2 n \tag{3}$$

with D the particle diffusivity. These equations are defined in a box $[-L_x, L_x] \times [-L_y, L_y]$, with aspect ratio $\epsilon = L_x/L_y$ and periodic boundary conditions. The system is driven by the equilibrium current density, $J_{eq}(x) = \cos(x)$ (having set $L_x = \pi$). Following standard techniques, we define the tearing mode stability parameter Δ'. For the considered equilibrium, $\Delta' = 2\kappa \tan \pi\kappa/2$, where $\kappa = \sqrt{1 - m^2\epsilon^2}$ and m is an integer. Tearing perturbations $\phi = \phi_L(x)e^{ik_y y}$, with $k_y = m\epsilon$, are linearly unstable when $\epsilon < 1$ ($\Delta' > 0$).

The linearized system can be solved analytically. For reasons of brevity, we omit the analytic derivation and present only a brief summary of the main interesting regimes.

$P = D = 0$

The tearing mode growth rate, $\gamma = \gamma_T$, is obtained also when $\omega_{*e} = k_y v_* = 0$. For sufficiently large values of ω_{*e}/γ_T, the mode becomes delocalized. Figure 1(a) shows an example of what happens to the perturbed current density during the initial growth of the instability for $\eta = 1 \times 10^{-4}$, $\Delta' = 0.71$ and $\omega_{*e}/\gamma_T = 3$.

$P \neq 0$

For non-zero values of the Prandtl number, a turning point is introduced in space beyond which the

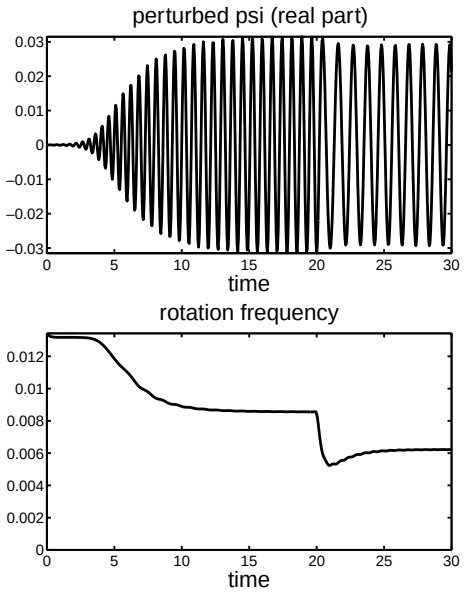

Figure 2. Non-linear evolution. Top: magnetic signal; bottom: rotation frequency.

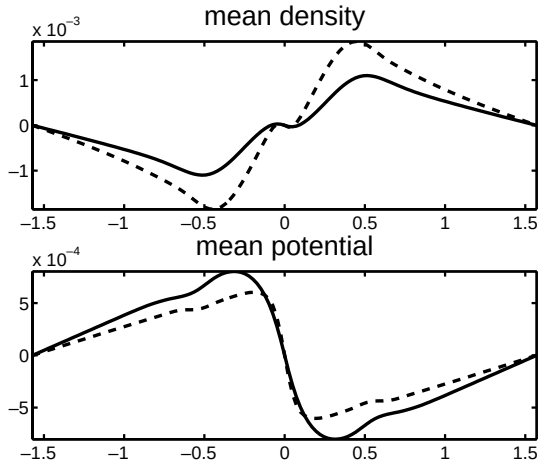

Figure 3. Mean fields, density and potential, for $D = 5 \times 10^{-5}$ (solid) and $D = 2.5 \times 10^{-5}$ (dashed).

eigenfunction decays exponentially to zero. When $\omega_{*e}/\gamma_T > 1$ and $\mu > \omega_{*e}^{7/3}(\Delta')^{-2/3}$, a new scaling for the growth rate is found, $\gamma \sim \Delta'^{6/5}\eta^{4/5}\omega_{*e}^{-1/5}P^{-1/5}$. An example of the eigenfunction for $P = 0.1$, $\eta = 1 \times 10^{-4}$, $\Delta' = 0.71$ and $\omega_{*e}/\gamma_T = 3$ is shown in Fig. 1(b). The mode is now localized with radial oscillations.

$D \neq 0$

The most striking effect on the mode structure is found for non-zero values of the diffusivity parameter. At $D/\eta \approx 10^{-2}$, the mode structure is localized even for $P = 0$; in addition, the radial oscillations are wiped out completely. The effect on the mode growth rate is negligible, as can be shown analytically. An example of the numerical solution is shown in Fig. 1(c), for $\eta = 10^{-4}$, $\Delta' = 0.405$, $\omega_{*e}/\gamma_T = 3$ and $D = 5 \times 10^{-6}$.

We also present preliminary non-linear studies of Eqs (1)–(3), aimed at identifying the interesting phenomenology. Figure 2 shows the evolution of the magnetic signal of the dominant mode and the rotation frequency. For this run, $\Delta' = 0.34$, $\eta = 1 \times 10^{-3}$, $P = 0.2$, $D = 5 \times 10^{-5}$ and $\omega_{*e} = 0.015$. The mode initially grows exponentially and rotates at the linear frequency $\omega_{lin} \approx 0.013$, but then it slows down to a somewhat lower frequency. This is accompanied by a reduction of the mean density gradient in the island region. Density flattening is caused by the electric field advection in the continuity Eq. (3) and is counterbalanced by the diffusivity. Figure 2 also shows that when the diffusivity is reduced to $D = 2.5 \times 10^{-5}$, as we do at time $t = 20$, the frequency drops further. Figure 3 shows the profiles of the mean fields for two values of diffusivity. We also find that the amplitude of the saturated island is only weakly affected by the diamagnetic frequency, being about 10% less than the amplitude obtained [4] with the RMHD model for the corresponding value of Δ'.

2. Neoclassical tearing modes

Neoclassical tearing modes can be destabilized in weakly collisional toroidal plasmas, as a consequence of the local reduction of the bootstrap current within a magnetic island of finite width in an otherwise stable equilibrium with $\Delta' < 0$ [5]. The local current reduction follows the quasi-linear pressure flattening within the island region. While the proposed theoretical models appear to be in qualitative agreement with experimental observation [6], non-linear diamagnetic effects, which as argued in the previous section are expected to play an important role, have not been properly included in the models. Furthermore, the critical threshold, in terms of the initial seed island for the onset of these modes, is still an open question [7–9]. These modes are deemed dangerous for a tokamak reactor because the critical seed island can be provided by error fields or through the coupling with sawteeth and other magnetic modes.

A number of suggested stabilization schemes rely on RF waves. These can be divided into two classes. The first class depends on global modifications of

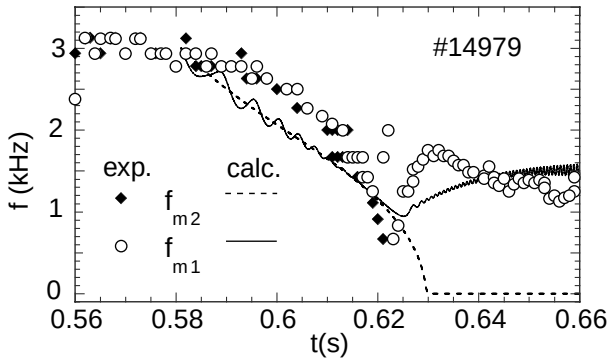

Figure 4. Time evolution of the frequencies of the oscillations with $m = 1$ and $m = 2$ poloidal mode numbers in FTU shot 14979. Diamonds correspond to $m = 2$ oscillations at $r \approx r_{q=2}$, circles to $m = 1$ oscillations at $r \approx r_{q=1}$; full and dashed lines show the results of the theoretical model in Ref. [13].

the background current density profile due to heating or considerable current drive. The second class relies on the subtler local balance between the RF driven current and the helical bootstrap current modification. In the latter case, the stabilization task requires that, in the frame of the rotating island, the externally applied counter-electromotive field, $E_{CD} = -\langle \partial \psi_{CD}/\partial t \rangle$, be seen as constant. Therefore, in the laboratory frame the source should be modulated in phase with the rotating island [10]. However, in recent experiments on ASDEX [11] and FTU [12], the much simpler scheme of unphased ECRH and ECCD on magnetic islands with helicity $m/n = 2/1$ was applied with success.

On FTU, the effect of ECRH on neoclassical islands was studied in detail. Experiments were performed with EC wave injection from the low field side, O mode polarization at the fundamental frequency, $f = 140$ GHz, and EC power $P_{EC} = 800$ kW. At low currents and high q values, $I_p \approx 350$ kA and $q_\psi \approx 6$, sawtooth oscillations were suppressed. With moderate reshaping of the current density profile induced by off-axis ECRH and increasing values of poloidal beta, the stability of MHD resistive modes with $m/n = 2/1$ was altered and temperature oscillations due to rotating magnetic islands were observed to grow.

The dynamics of coupled rotating magnetic islands associated with ECRH can be interpreted on the basis of non-linear model equations, given in detail in Ref. [13], which describe the interaction of the island inertia with the resistive wall braking torque and the electrodynamic coupling of the mode side bands. Coupling can have a stabilizing or destabilizing effect, depending on the phase difference $\Delta\phi$, which evolves non-linearly in a pendulum-like fashion. During an ECRH pulse in FTU, e.g. shot 14979 shown in Fig. 4, the $m/n = 1/1$ and $m/n = 2/1$ magnetic islands initially rotate at a common frequency controlled by the larger of the two islands. This frequency is occasionally seen to jump between the natural frequencies, which, in the plasma rest frame, are related to the electron diamagnetic frequencies at the corresponding mode rational surfaces. This frequency jump is the result of the competition between the mutual torques associated with the two islands, viscous drag and wall braking. In Fig. 4, for $t < 0.62$ s, the $m/n = 2/1$ island is the larger and determines the common rotation frequency, $\omega(t) \sim \omega_{*e}(r_2)$, where $q(r_2) = 2$. This frequency slows down as a consequence of the interaction with the resistive wall. Decoupling of the two islands occurs at $t = 0.62$ s, when $\omega(t)$ reaches a value close to $\omega_{*e}(r_1)$. Superimposed on the experimental points is the result of a numerical simulation based on our model. Theoretically, mode decoupling is an important new result that follows the non-linear behaviour of the phase difference $\Delta\phi$, since the coupling torque depends to a considerable extent on this phase difference.

3. Model for the sawtooth period and amplitude

Sawtooth crashes are triggered by internal kink modes with toroidal $n = 1$ and dominant poloidal $m = 1$ mode numbers (in short, an $m = 1$ mode) [14, 15]. The necessary instability condition for these modes is that q drop below unity in the central plasma region. However, it is clear from both theory and experiments that consideration of non-ideal MHD effects is necessary in order to understand sawtooth behaviour, particularly the threshold for reconnection and the resulting sawtooth period and amplitude. This threshold can be written as [16]

$$\delta W < \delta W_{crit} \qquad \text{for instability} \tag{4}$$

where

$$\delta W = \delta W_{mhd} + \delta W_{KO} + \delta W_{fast} \tag{5}$$

is an effective potential energy functional, with δW_{mhd} the ideal MHD part [17, 18], δW_{KO} the part contributed by the thermal trapped ions (the Kruskal–Oberman contribution) [19, 20], δW_{fast} the

fast particle contribution [21, 22] and δW_{crit} a critical threshold determined by microscopic effects (i.e. electron–ion collisions, ion Larmor radius, electron skin depth, diamagnetic frequency, etc.) in a narrow layer around the $q = 1$ surface, where reconnection of magnetic field lines can occur. Detailed expressions for δW and δW_{crit} can be found in Ref. [16].

The fast particle contribution δW_{fast} is responsible for the 'monster sawteeth', which first appeared in JET discharges where a fast ion population was created by ICRH. Monsters are actually periods of transient sawtooth stabilization lasting a fraction of the global resistive diffusion time, more precisely, the time for the $q = 1$ radius r_1 to evolve to about 50% of the plasma minor radius, starting from a sawtooth relaxed q profile; at these large values of r_1, fast ion sawtooth suppression becomes ineffective. To the extent that the resistive diffusion time is much longer than the energy confinement time, the central temperature saturates during the sawtooth free period until a giant crash occurs, giving rise to the characteristic shape of monster X ray traces.

Another important ingredient associated with the stability criterion (5) is the local magnetic shear. For most tokamak discharges of interest today, including those of TCV and FTU, the relevant layer physics determining the δW_{crit} threshold term corresponds to the 'ion kinetic regime' [23], where electron–ion collisions determine the impedance to the parallel electric field in the reconnection layer, but the ion Larmor radius is comparable to or larger than this layer; in addition, diamagnetic effects are important. Under these circumstances, the instability condition (4) is equivalent to [24]

$$\max(\gamma_\rho, \gamma_\eta) > c_*(\omega_{*e}\omega_{*i})^{1/2} \tag{6}$$

where γ_ρ and γ_η are the ion kinetic [23] and resistive kink [15] growth rates, respectively, c_* is a numerical factor of order unity and the diamagnetic frequencies are evaluated at r_1. This condition can be recast in terms of a critical magnetic shear condition for the local parameter $s_1 = r_1 q'(r_1)$, as is done in Ref. [16]. For the case $\gamma_\rho > \gamma_\eta$

$$s_1 > s_{1,crit} = c_*^{7/6}\,[\pi T_i/2(T_i + T_e)]^{1/3} \times \tau_A^{7/6}(\omega_{*e}\omega_{*i})^{7/12}(r_1/\rho_i)^{2/3}S^{1/6} \tag{7}$$

where τ_A is the relevant Alfvén time, ρ_i is the ion Larmor radius and S is the magnetic Reynolds number.

The sensitivity to the local magnetic shear was tested in JET discharges with fast wave current drive, where phasing of the ICRH antennas led to lengthening or shortening of the sawtooth period, depending on the sign of the driven current, when the resonant absorption layer was close to the $q = 1$ radius [25].

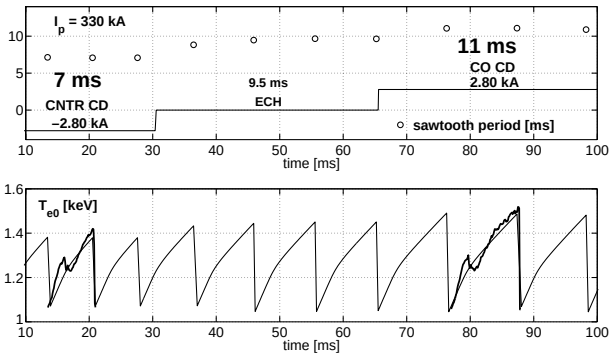

Figure 5. TCV sawtooth simulations of shots 15278 and 15282. Top: ECCD as a function of time; bottom: central electron temperature. Also shown in the bottom panel are two experimental soft X ray sawtooth traces.

Various experiments performed on TCV have highlighted the strong sensitivity of the sawtooth period to ECH and ECCD operation conditions [26, 27]. Simulations performed with the PRETOR code, where the sawtooth crash trigger criterion discussed in this section has been implemented, are in good agreement with the experimental results [28]. In Fig. 5, we present in more detail the simulation of a dedicated experiment showing the influence of even small amounts of current drive close to the $q = 1$ surface on the sawtooth period. Two shots with identical plasma conditions have been produced [27]: in one case, shot 15278, the ECH power is accompanied by a small amount of counter-CD (less than 1% of the plasma current); in the second case, shot 15282, the same power deposition is accompanied by a similar amount of co-CD. The sawtooth period changes experimentally from 7 to 11 ms. A simulation performed fitting the c_* coefficient in Eq. (7) to the ohmic sawtooth period reproduces the observed trends. As the ECH power deposition is nearly the same in the two cases, the simulated critical shear is the same function of time for the two discharges. In contrast, the small amount of CD, well localized close to the $q = 1$ surface, changes the evolution of the magnetic shear at $q = 1$, i.e. s_1 increases more quickly after a crash with counter-CD and more slowly with co-CD. Thus the time to cross the threshold in Eq. (7) is different for the two cases, changing the sawtooth period in very good agreement with the experimental data.

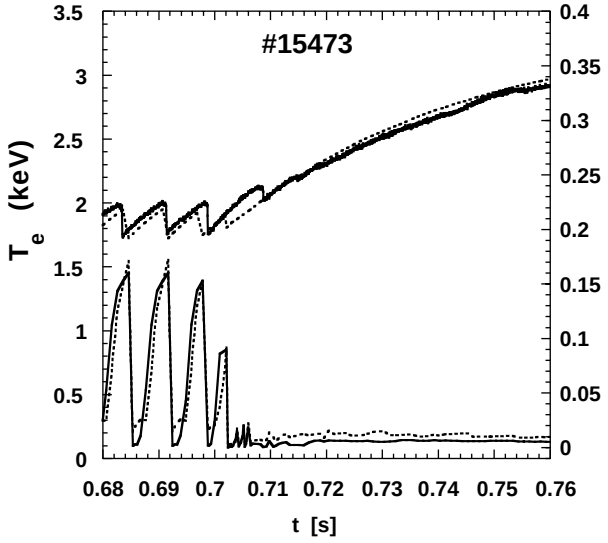

Figure 6. FTU shot 15473. Upper traces: experimental (solid line) and simulated (dotted line) time evolution of the central electron temperature; lower traces: $s_1(t)$ (dotted line) and $s_{1,crit}(t)$ (solid line).

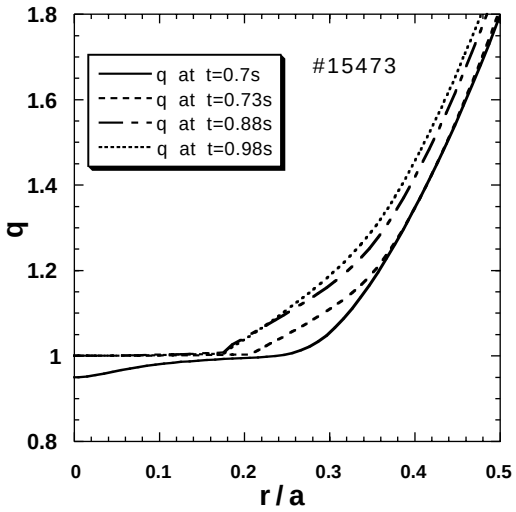

Figure 7. FTU shot 15473. Simulated q profile at various times, starting from the time of ECRH switch-on, $t = 0.7$ s.

Next we present a comparison of FTU experimental results with simulations obtained with a 1-D transport code, where the sawtooth trigger model (7) has been implemented [29]. When Eq. (7) is satisfied, the q profile is relaxed following Kadomtsev's full reconnection prescription [14]. Density and temperature profiles are flattened up to Kadomtsev's mixing radius, while conserving particle number and energy.

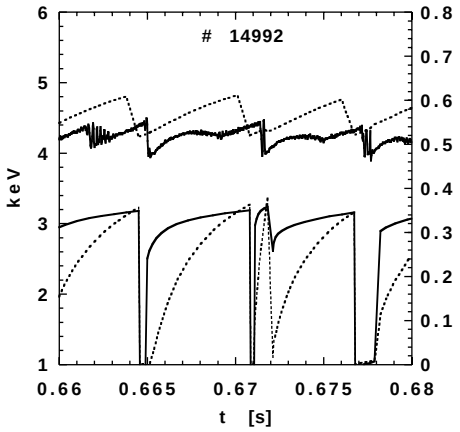

Figure 8. FTU shot 14992 with co-ECCD applied near $q = 1$. Upper and lower traces: same as in Fig. 6.

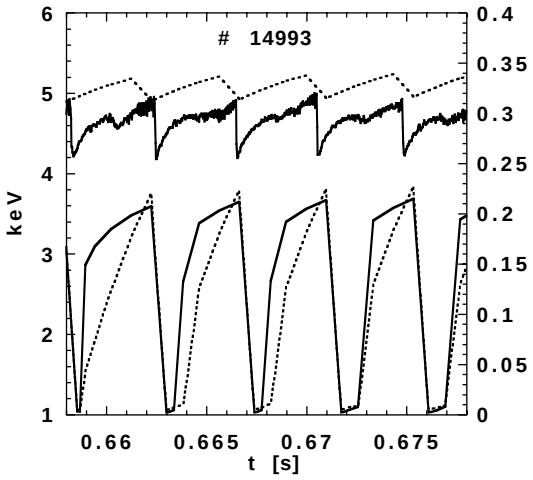

Figure 9. FTU shot 14993 with counter-ECCD applied near $q = 1$. Upper and lower traces: same as in Fig. 6.

Figures 6 and 7 illustrate the numerical simulation of FTU discharge 15473, where ECRH is applied near the $q = 1$ surface at time $t \approx 0.7$ s. The effect of localized heating is that of shrinking the $q = 1$ radius, reducing both the local and the critical magnetic shear values. For $t > 0.7$ s, the electron temperature rises, and small and rapid sawteeth still occur, which, however, now involve a narrow central region within which the temperature profile is nearly flat. Comparisons between simulated and experimental sawtooth traces are shown in Fig. 8 for FTU shot 14992, with applied co-ECCD, and in Fig. 9 for FTU shot 14993, with applied counter-ECCD, at $t \approx 160$ ms after EC switch-on. As compared with the ohmic phases of the same discharges, we find that co-CD increases the sawtooth period, while

counter-CD leaves it practically unchanged, probably because of the low counter-current level achieved and the competing destabilizing effect of heating. These effects are also well described by the adopted sawtooth model.

The satisfactory agreement between the observed sawtooth periods in ohmic and ECRH discharges in TVC and FTU and the simulation results indicate that the adopted sawtooth model is capable of capturing the main trends, i.e. variations of the sawtooth period when operation conditions are changed. However, the period itself can be predicted only within a factor of 2 uncertainty. Nevertheless, the agreement is remarkable, especially in view of the fact that the sawtooth trigger model is based on linear stability theory, while magnetic fluctuations are often observed in ECRH experiments, superimposed over a significant fraction of sawtooth ramps, indicative of the presence of saturated, $m/n = 1/1$ magnetic islands with an amplitude exceeding the reconnection layer width expected from linear theory. A possible explanation is that, indeed, linear theory indicates that m/n=1/1 drift tearing modes may be unstable during sawtooth ramps when inequality (4) is reversed, giving rise to low amplitude magnetic islands; however, a full sawtooth crash requires a more virulent instability whose threshold is consistent with Eqs (4) and (6). A model for the dynamics of saturated $m/n = 1/1$ magnetic islands during ECRH has been proposed in Ref. [30].

4. Temperature profiles during sawteeth and localized ECRH

A model for the evolution of the electron temperature profile during localized ECRH and sawtooth activity has been proposed recently [31]. The model solves the electron thermal energy diffusion equation, taking into account the anisotropy introduced by the magnetic field (heat diffusion along field lines is much faster than cross-field diffusion), a localized heat source, plasma rotation and, most importantly, the appropriate magnetic topology corresponding to the growth of an $m/n = 1$, macroscopic magnetic island. A helical flux function is introduced, $\psi_* = \psi_*(r, \theta - \phi; \xi)$, where θ and ϕ are the poloidal and toroidal angles, respectively, and $\xi = \xi(t)$ is the radial displacement of the hot core magnetic axis as a function of time. Figure 2 of Ref. [31] illustrates a poloidal cross-section of the $\psi_* = $ const flux surfaces and the heating region of

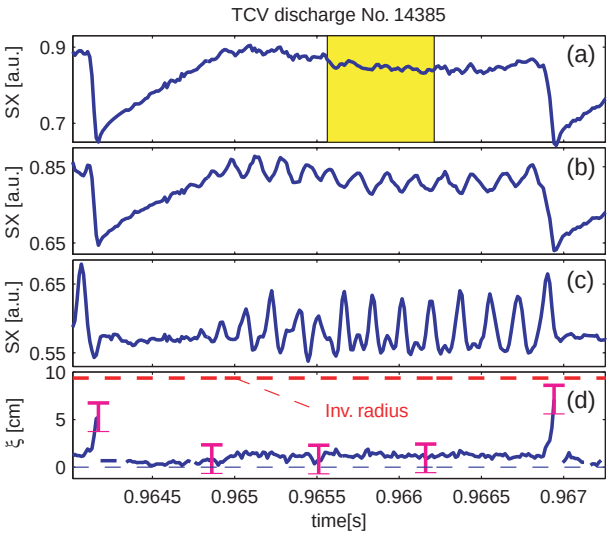

Figure 10. TCV saturated sawtooth. Temporal traces of soft X ray emissivity along chords at different radial distances r_X from the magnetic axis. $r_X \approx$ (a) $0.02r_{inv}$, (b) $0.28r_{inv}$ and (c) $0.9r_{inv}$. The measured displacement function $\xi(t)$ is shown in (d), together with the position of the inversion radius (dashed line).

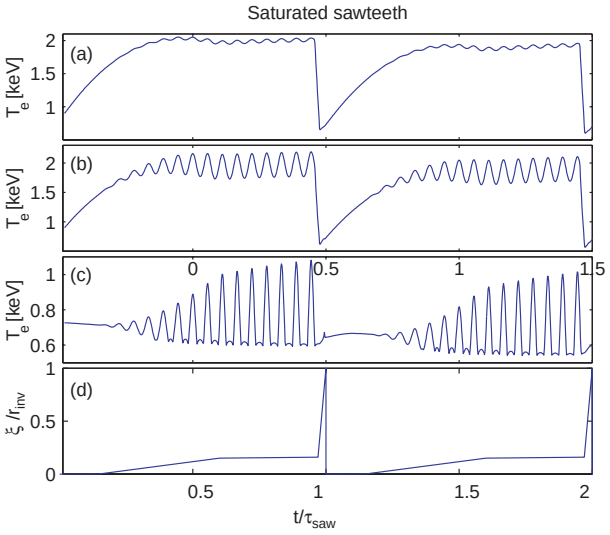

Figure 11. M1TEV simulation of the soft X ray traces shown in Fig. 10. The time is normalized to the sawtooth period τ_{saw}. The displacement function used in the simulation, normalized to the inversion radius, is shown in (d).

the ECRH. The deposited ECRH power is effectively spread along an annular region as a consequence of large parallel thermal conduction and plasma rotation. The diffusion equation, which is defined in a Lagrangian frame, basically describes the evolution

of electron thermal energy on magnetic flux tubes frozen to the plasma flow. Advection of the flux tubes is consistent with internal kink flow cells, which are parameterized by $\xi(t)$. At the particular instant in time when two flux surfaces reconnect, a mixing rule for the thermal energy is implemented [31]. The simulation code that evolves the electron temperature according to the rules outlined above has been given the name M1TEV. More details of the simulation code can be found in Ref. [32].

The first application [31] of M1TEV was finalized for the interpretation of the temperature filamentary structures observed in RTP [33] and TEXT-U [34] experiments during intense localized ECRH. These multipeaked temperature profiles are obtained by M1TEV assuming an ECRH deposition width narrower than the size of the $m/n = 1$ island, which in these experiments is observed to grow slowly during sawtooth ramps.

A second application [35] was aimed at the interpretation of the 'humpback' relaxation oscillations, first observed in T-10 [36] and later reported by the TCV team [37] with intense ECRH near the $q = 1$ radius. The distinctive feature of humpback relaxations is the fast drop and rise of the central soft X ray emissivity, on a timescale normally below 1 ms in TCV. Our interpretation of the humpback phenomenon, as supported by M1TEV code simulations, is based on the following two ingredients. First, intense localized ECRH near $q = 1$ can produce electron temperature profiles that are nearly flat in the centre, up to the $q = 1$ radius, and then fall steeply beyond that radius. Secondly, once these profiles are produced prior to the sawtooth relaxation phase, the fast development of an m/n=1 magnetic island and the corresponding advection and mixing of electron thermal energy cause the fast drop and rise of the soft X ray line integrated intensity.

In the M1TEV model, the displacement function $\xi(t)$ is a free parameter, not determined theoretically. An effort has been made to infer this function from TCV experimental data by measuring as a function of time the radial distance of the peak of the soft X ray emissivity profile from its initial position at the bottom of the sawtooth ramp. An example is shown in Fig. 10, illustrating a saturated sawtooth obtained in TCV discharge 14385 during slightly off-axis ECRH (deposited mostly well within the sawtooth inversion radius). In particular, Fig. 10(d) shows the measured displacement function. When this function is used in M1TEV together with the appropriate values of the relevant input parameters, the simulated sawtooth traces shown in Fig. 11 are obtained. Other examples of simulated TCV sawteeth can be found in Ref. [32].

5. Collisionless magnetic reconnection

Magnetic field line reconnection in high temperature plasmas is one of the most fertile problems in physics owing to its relevance to astrophysical and laboratory plasmas and to its theoretical implications. One of its most important features is the interplay between the energetic and the topological aspects that characterize its evolution: a local relaxation of the topological magnetic structure is accompanied by a fast release of magnetic energy. This energy is transformed into ion kinetic motion, into internal (compressional) electron energy, and into either heat (dissipative reconnection) or ordered electron kinetic energy (Hamiltonian reconnection) [38].

Research on magnetic reconnection in collisionless plasmas was originally motivated by applications to space plasma processes, such as reconnection events occurring in the Earth's magnetotail (see, for example, Ref. [39]). Renewed interest in this problem was prompted by the observation of fast sawtooth relaxations in JET. Wesson [40], using a semi-heuristic Sweet–Parker type of argument, was the first to point out that electron inertia may account for the observed fast relaxation time $\tau_{crash} \approx 50$ μs. More detailed analytic and numerical work [41–43] showed that: (i) The actual fast reconnection timescale in JET relevant regimes, τ_{rec}, is determined by a combination of the electron skin depth d_e and the ion (sound) gyroradius ρ_s, namely $\tau_{rec} \sim \tau_A(r_1/d_e)(d_e\rho_s)^{2/3}$, which gives values of τ_{rec} close to τ_{crash} for JET parameters. (ii) The structure of the collisionless reconnection region is very different from that associated with the classic, collisional Sweet–Parker process.

An appropriate model for collisionless reconnection is Eq. (1), with $\mu = 0$, and the collisionless version of Ohm's law

$$\frac{\partial F}{\partial t} + [\varphi, F] = \rho_s^2[U, \psi] \tag{8}$$

where $F = \psi + d_e^2 J$ is the velocity space averaged canonical momentum along the ignorable z direction. The term proportional to ρ_s^2 represents electron compressional effects, which are important insofar as $\rho_s > d_e$. Equations (1) (with $\mu = 0$) and (8), together with $U = \nabla^2\phi$ and $J = -\nabla^2\psi$, are

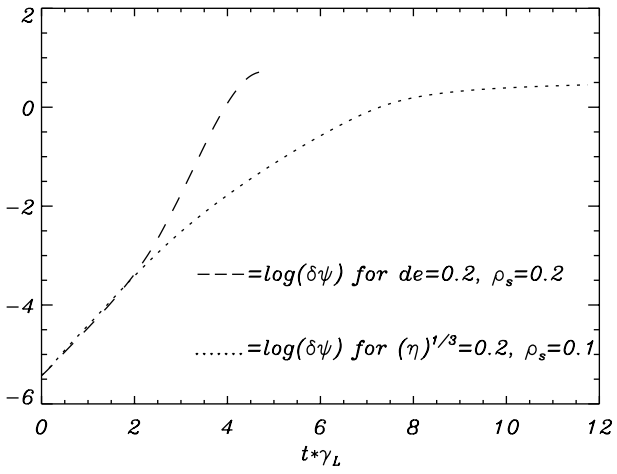

Figure 12. Normalized growth time of the logarithm of the island width in the collisionless $d_e = \rho_s = 0.2$ case (solid line) and in the resistive $d_e = 0$, $\rho_s = 0.1$ and $\eta^{1/3} = 0.2$ case (dashed–dotted line). Time runs along the horizontal axis.

a closed set. In Refs [42, 43], these equations were solved in a planar slab subject to double periodic boundary conditions. Choosing a slab aspect ratio $\epsilon = 0.5$ and values of d_e and ρ_s such that $\Delta'(0.5)d_e > (d_e/\rho_s)^{1/3}$, a quasi-explosive non-linear growth was found on the timescale τ_{rec} indicated above, although the adopted boundary conditions limited the interesting non-linear phase to island widths smaller than the box size (see also Ref. [44]).

More recently, we have solved the same set of equations removing the double periodic boundary conditions. We have adopted a Harris pinch equilibrium, $B_{eq} = B_0 e_z + B_{yeq}(x)e_y$, where $B_{yeq}(x) = \tanh(x/L)$ and L is the equilibrium scale length. This equilibrium is unstable to tearing perturbations, periodic in y over the distance L_y, when $L < \pi L_y$. In the x direction, we impose the condition that the fields ϕ and $\psi - \psi_{eq}$ vanish at infinity. The linear (small perturbation) phase can be solved analytically. In the limit $\Delta' \to \infty$, the normalized growth rate [41] $\gamma_L \approx (2d_e\rho_s^2/\pi)^{1/3}$ is recovered. With the Harris pinch configuration, a single coherent magnetic island can now be followed in time, until its width saturates at a macroscopic amplitude.

The non-linear evolution requires numerical work. Equations (1) (with $\mu = 0$) and (8) are solved on a non-uniform mesh with an increasing density of grid points in the central region. The integration domain is limited to large values of x, such that the boundary fluxes are negligible. A suitable filtering of the small spatial scale lengths (well below the electron skin depth) has been included which is capable of ensuring numerical stability while not altering the required conservation properties significantly. The solution is compared with a purely resistive case. Choosing the parameters for two comparison runs such that the collisionless and the resistive linear growth rates are the same, the collisionless case exhibits a faster, quasi-explosive non-linear growth that we are now able to follow to saturation (Fig. 12). Thus we confirm the result in Refs [42, 43], indicating that the magnetic island grows to a macroscopic amplitude on the timescale $\tau_{rec} \sim \gamma_L^{-1}$. By contrast, the resistive simulation shows that the non-linear growth takes place on the Sweet–Parker timescale, $\tau_{SW} \sim (\tau_\eta \tau_A)^{1/2}$. Interestingly, the saturation level for the two cases is nearly the same.

The collisionless model we have adopted admits two families of topologically invariant fields

$$G_\pm = F \pm d_e \rho_s U. \tag{9}$$

Equations (1) and (8) can be written as

$$\frac{\partial G_\pm}{\partial t} + [\varphi_\pm, G_\pm] = 0 \tag{10}$$

where $\varphi_\pm = \varphi \pm (\rho_s/d_e)\psi$. The energy functional playing the role of the system Hamiltonian [45] is

$$H = -\frac{1}{2}\int d^2x(\varphi_+ G_+ + \varphi_- G_-). \tag{11}$$

Equations (10) explicitly show the Lagrangian conservation of the fields $G_\pm$, advected by the generalized flows $v_\pm = e_z \times \nabla\varphi_\pm$. Clearly, any function of $G_\pm$ is also a conserved field. It was shown in Ref. [43] that the existence of these topological invariants is responsible for the structure of the reconnection region, in particular the cross-shaped structure of the current density and vorticity layers and the generation of microscales below the electron skin depth. A more general question of principle that we address here (see also Ref. [38]) is how to reconcile the reversible energy transport to small scales implied by the dissipationless reconnection evolution, with the seemingly irreversible approach to a saturated equilibrium with a macroscopic magnetic island.

The resolution of this apparent paradox is phase mixing of the Lagrangian invariants, i.e. the functions $G_\pm$ develop fine scale oscillations as they are advected by vortical patterns corresponding to the velocity fields $v_\pm$, while the functions ϕ and ψ, which can be expressed through integrals of $G_\pm$, turn out to be smooth. This process can be more easily understood in terms of a formal analogy with the standard

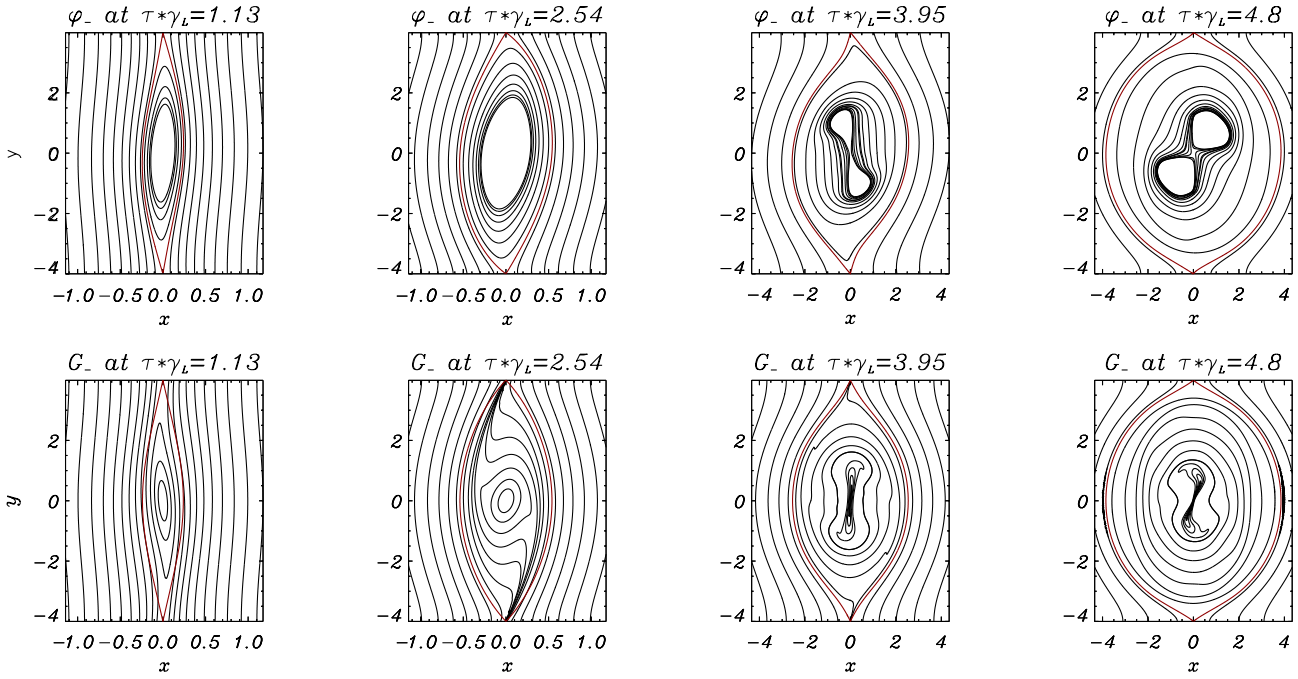

Figure 13. In the first row the contour levels of the single particle Hamiltonian φ_- at different simulation times are plotted. The separatrices are superimposed in red. In the second row the contour levels of the Lagrangian invariant G_- are drawn (the red contour is the island separatrix). Note that the scale in the x direction is different at later times.

Vlasov–Poisson problem for electrostatic Langmuir waves [46]. The set of Eqs (10) has the form of two coupled 1-D Vlasov equations, with x and y playing the role of the co-ordinate and the conjugate momentum for the 'distribution functions' $G_\pm$ of two 'particle' species with equal charges in the Poisson-like equation for ϕ,

$$d_e \rho_s \nabla^2 \phi = (G_+ - G_-)/2 \tag{12}$$

and opposite charges in the Yukawa-type equation for ψ,

$$\psi - d_e^2 \nabla^2 \psi = (G_+ + G_-)/2 \tag{13}$$

The generalized stream functions $\phi_\pm$ play the role of the single particle Hamiltonians. Thus, similarly to Bernstein–Green–Kruskal (BGK) [47] solutions, the stationary solutions of Eqs (10) can be written in the form $G_\pm = \mathcal{G}(\phi_\pm)$ (there is a single function $\mathcal{G}$ because of the symmetry relation $G_+(-x, y) = G_-(x, y)$). However, the present problem and the standard Vlasov–Poisson problem are not formally identical. In Poisson's equation, the source term is the electron density, which is the velocity space integral of the distribution function and as such does not exhibit fine scale oscillations. In our problem, the source terms for Eqs (12) and (13) are the distribution functions $G_\pm$ themselves. On the other hand, the fields ϕ and ψ, the solutions of these equations, can be expressed in terms of integrals of $G_\pm$. Thus the fine scale structure of $G_\pm$ does not show up in ϕ and ψ. An illustration of this process is the numerical solution shown in Fig. 13.

In this fully non-linear phase, a new characteristic dynamical time related to the eddy turnover time of the Lagrangian invariants inside the island becomes of interest. When this turning time, which decreases as the instability grows, becomes of the order of the non-linear island growth time, energy is removed effectively from the large spatial scales leading to the island growth saturation. The phase mixing of the Lagrangian invariants can allow the plasma to access a new 'macroscopic' stationary state without violating energy conservation. This process leads to the formation of macroscopic BGK equilibria [47], superimposed on increasingly thin filaments, as in the case of the non-linear Landau damping of Langmuir waves. This can be seen by separating the Lagrangian invariants into coarse grained and phase mixed parts and by noticing that, in the spatial integration that gives ψ and φ from $G_\pm$, the contribution of the phase mixed small scale filaments of $G_\pm$ averages out. On the other hand, these small scale structures continue to contribute to total energy

conservation through the quadratic $d_e^2 J^2$ and $\rho_s^2 U^2$ terms in Eq. (14). On the basis of this separation, it was shown in Ref. [38] that the macroscopic magnetic equilibrium can be cast in the form $\bar{J} = \mathcal{F}(\bar{\psi})$, where a bar denotes coarse grained quantities and $\mathcal{F}$ is an arbitrary function, which need not contain either d_e or ρ_s, consistently with the fact that the saturated island widths are comparable for collisionless and resistive regimes.

6. Conclusions

In this article, we have presented recent advances in the understanding of macroscopic island dynamics in magnetized plasmas, made possible by a profitable interaction between theory and experiments. The understanding, however, is still far from complete. The main conclusions from our analysis can be summarized as follows:

(1) A satisfactory model for the sawtooth period and amplitude has been developed and validated against TCV and FTU experiments. The model points to the importance of diamagnetic effects, which introduce a threshold for the trigger of the sawtooth crash in terms of a critical value of the local magnetic shear parameter. Localized current drive can influence the time evolution of the local magnetic shear and thus represents an effective means for sawtooth control. The model also includes the effect of fast ions, which in previous work were shown to explain the long monster sawtooth periods observed in JET. Thus the proposed sawtooth model is a state of the art viable tool for predicting sawtooth behaviour in future experiments, and as such it has been implemented in predictive transport codes such as PRETOR and BALDUR.

(2) Diamagnetic effects are important not only for the determination of the linear stability threshold of $m/n = 1$ modes. Neoclassical magnetic islands in FTU are observed to rotate at the electron diamagnetic frequency. A non-linear model for the dynamics of coupled rotating magnetic islands has been developed and compared with FTU data. In another theoretical development, preliminary results on the evolution of non-linear drift tearing modes, based on a reduced three field model, have been presented. It is shown that density gradients in the reconnection region can be maintained non-linearly and give rise to diamagnetic rotation of macroscopic magnetic islands.

(3) A model for the evolution of electron temperature profiles during sawteeth and localized ECRH has been developed and compared against TCV and FTU data.

(4) In large size tokamaks such as JET, sawtooth reconnection can occur under nearly collisionless conditions. We have shown that non-linear collisionless reconnection is fast enough to account for the observed relaxation time in JET sawteeth. We have also shown that the growth and saturation of magnetic islands can occur in collisionless conditions. Irreversibility in collisionless reconnection is associated with the phase mixing of conserved fields. In this sense, magnetic island saturation has a formal analogy with the formation of BGK equilibria for dissipationless Langmuir waves.

References

[1] Ara, G., et al., Ann. Phys. (N.Y.) **112** (1978) 443.
[2] Furth, H.P., Killeen, J., Rosenbluth, M.N., Phys. Fluids **6** (1963) 459.
[3] Bussac, M.N., Edery, D., Pellat, R., Soule, J.L., Phys. Rev. Lett. **40** (1978) 1500.
[4] Tebaldi, C., Ottaviani, M., Porcelli, F., Plasma Phys. Control. Fusion **38** (1996) 619.
[5] Hegna, C.C., Callen, J.D., Phys. Fluids B **4** (1992) 4072.
[6] Sauter, O., et al., Phys. Plasmas **4** (1997) 1654.
[7] Smolyakov, A.I., et al., Phys. Plasmas **2** (1995) 1581.
[8] Wilson, H.R.J., et al., Plasma Phys. Control. Fusion **38** (1996) A149.
[9] Waelbroeck, F.L., Fitzpatrick, R., Phys. Rev. Lett. **78** (1997) 1703.
[10] Buttery, R., in Controlled Fusion and Plasma Physics (Proc. 26th Eur. Conf. Maastricht, 1999), Vol. 23J, European Physical Society, Geneva (1999) 121.
[11] Zohm, H., et al., Nucl. Fusion **39** (1999) 577.
[12] Cirant, S., et al., in Fusion Energy 2000 (Proc. 18th Int. Conf. Sorrento, 2000), IAEA, Vienna (2001) CD-ROM file EX3/3 and http://www.iaea.org/programmes/ripc/physics/start.htm.
[13] Lazzaro, E., et al., Phys. Rev. Lett. **84** (2000) 6038.
[14] Kadomtsev, B.B., Fiz. Plazmy **1** (1975) 710; Sov. J. Plasma Phys. **1** (1975) 389.
[15] Coppi, B., et al., Fiz. Plazmy **2** (1976) 961; Sov. J. Plasma Phys. **2** (1976) 533.
[16] Porcelli, F., Boucher, D., Rosenbluth, M.N., Plasma Phys. Control. Fusion **38** (1996) 2163.
[17] Bussac, M.N., Pellat, R., Edery, D., Soule, J.L., Phys. Rev. Lett. **35** (1975) 1638.
[18] Lütjens, H., Bondeson, A., Vlad, G., Nucl. Fusion **32** (1992) 1625.
[19] Kruskal, M.D., Oberman, C.R., Phys. Fluids **1** (1958) 275.

[20] Fogaccia, G., Romanelli, F., Phys. Plasmas **2** (1995) 227.
[21] Porcelli, F., Plasma Phys. Control. Fusion **33** (1991) 1601.
[22] Coppi, B., Migliuolo, S., Pegoraro, F., Porcelli, F., Phys. Fluids B **2** (1990) 927.
[23] Pegoraro, F., Porcelli, F., Schep, T.J., Phys. Fluids B **1** (1989) 364.
[24] Sauter, O., et al., in Theory of Fusion Plasmas (Proc. Joint Varenna–Lausanne Int. Workshop, Varenna, 1998).
[25] Bhatnagar, V.P., Nucl. Fusion **34** (1994) 1579.
[26] Goodman, T.P., et al., in Controlled Fusion and Plasma Physics (Proc. 26th Eur. Conf. Maastricht, 1999), Vol. 23J, European Physical Society, Geneva (1999) 1101.
[27] Henderson, M.A., et al., Fusion Eng. Des. (in press).
[28] Angioni, C., et al., in Proc. Joint Varenna–Lausanne Int. School of Plasma Physics Conf. Varenna, 2000, Editrice Compositori, Bologna (in press).
[29] Ramponi, G., et al., in Proc. 13th Topical Conf. on Radio Frequency Power in Plasmas, Annapolis, 1999, AIP Conf. Proc. **485** (1999) 265.
[30] Cirant, S., et al., Plasma Phys. Control. Fusion **41** (1999) B351.
[31] Porcelli, F., Rossi, E., Cima, G., Wootton, A., Phys. Rev. Lett. **82** (1999) 1485.
[32] Furno, I., et al., Nucl. Fusion **41** (2001) 403.
[33] Lopes Cardozo, N.J., et al., Phys. Rev. Lett. **73** (1994) 256.
[34] Cima, G., et al., Plasma Phys. Control. Fusion **40** (1998) 1149.
[35] Porcelli, F., et al., Nucl. Fusion **40** (2000) 1691.
[36] Razumova, K.A., et al., Plasma Phys. Rep. **23** (1997) 13.
[37] Pietrzyk, Z.A., et al., Nucl. Fusion **39** (1999) 587.
[38] Grasso, D., Califano, F., Pegoraro, F., Porcelli, F., Phys. Rev. Lett. **86** (2001) 5051.
[39] Vasyliunas, V.M., Rev. Geophys. Space Phys. **13** (1975) 303.
[40] Wesson, J.A., Nucl. Fusion **30** (1990) 2545.
[41] Porcelli, F., Phys. Rev. Lett. **66** (1991) 425.
[42] Ottaviani, M., Porcelli, F., Phys. Rev. Lett. **71** (1993) 3802.
[43] Cafaro, E., Grasso, D., Pegoraro, F., Porcelli, F., Saluzzi, A., Phys. Rev. Lett. **80** (1998) 4430.
[44] Lazzaro, E., Ferrero, M., Gianoli, L., Valdettaro, L., Phys. Scr. **61** (2000) 624.
[45] Kuvshinov, B.N., Lakhin, V., Pegoraro, F., Schep, T.J., J. Plasma Phys. **59** (1998) 4.
[46] O'Neil, T., Phys. Fluids **8** (1965) 2255.
[47] Bernstein, I.B., Greene, J.M., Kruskal, M.D., Phys. Rev. Lett. **108** (1957) 546.

(Manuscript received 8 October 2000
Final manuscript accepted 10 April 2001)

E-mail address of F. Porcelli:
porcelli@polito.it

Subject classification: C0, Te; C0, Ti; E0, Ti